



Experimental Research

Automated surgical workflow identification by artificial intelligence in laparoscopic hepatectomy: Experimental research

Kimimasa Sasaki^{a,b,c}, Masaaki Ito^{a,*}, Shin Kobayashi^b, Daichi Kitaguchi^a, Hiroki Matsuzaki^a, Masashi Kudo^b, Hiro Hasegawa^a, Nobuyoshi Takeshita^a, Motokazu Sugimoto^b, Shuichi Mitsunaga^{c,d}, Naoto Gotohda^{b,c}

^a Surgical Device Innovation Office, National Cancer Center Hospital East, 6-5-1, Kashiwanoha, Kashiwa-City, Chiba, 277-8577, Japan

^b Department of Hepatobiliary and Pancreatic Surgery, National Cancer Center Hospital East, 6-5-1, Kashiwanoha, Kashiwa-City, Chiba, 277-8577, Japan

^c Course of Advanced Clinical Research of Cancer, Juntendo University Graduate School of Medicine, 2-1-1, Hongo, Bunkyo-Ward, Tokyo, 113-8421, Japan

^d Department of Hepatobiliary and Pancreatic Oncology, National Cancer Center Hospital East, 6-5-1, Kashiwanoha, Kashiwa-City, Chiba, 277-8577, Japan

ARTICLE INFO

Meeting presentation: Presented at the 32nd Meeting of the Japanese Society of Hepato-Biliary-Pancreatic Surgery, Virtual, March 2021

Keywords:

Real-time surgical step identification
Computer vision
Laparoscopic hepatectomy
Convolutional neural network
Deep learning
Artificial intelligence

ABSTRACT

Background: To perform accurate laparoscopic hepatectomy (LH) without injury, novel intraoperative systems of computer-assisted surgery (CAS) for LH are expected. Automated surgical workflow identification is a key component for developing CAS systems. This study aimed to develop a deep-learning model for automated surgical step identification in LH.

Materials and methods: We constructed a dataset comprising 40 cases of pure LH videos; 30 and 10 cases were used for the training and testing datasets, respectively. Each video was divided into 30 frames per second as static images. LH was divided into nine surgical steps (Steps 0–8), and each frame was annotated as being within one of these steps in the training set. After extracorporeal actions (Step 0) were excluded from the video, two deep-learning models of automated surgical step identification for 8-step and 6-step models were developed using a convolutional neural network (Models 1 & 2). Each frame in the testing dataset was classified using the constructed model performed in real-time.

Results: Above 8 million frames were annotated for surgical step identification from the pure LH videos. The overall accuracy of Model 1 was 0.891, which was increased to 0.947 in Model 2. Median and average accuracy for each case in Model 2 was 0.927 (range, 0.884–0.997) and 0.937 ± 0.04 (standardized difference), respectively. Real-time automated surgical step identification was performed at 21 frames per second.

Conclusions: We developed a highly accurate deep-learning model for surgical step identification in pure LH. Our model could be applied to intraoperative systems of CAS.

1. Introduction

Laparoscopic hepatectomy (LH) was first reported in 1991 [1], with the first international consensus conference on LH held in 2008 in Louisville [2]. Since then, the number of LHs performed has significantly increased. More than 5000 LHs were performed in 2017 for both benign and malignant indications in Japan [3]. Regarding potential benefits [4, 5], LH reduces intraoperative blood loss, transfusion rate, postoperative morbidity, length of hospital stay [6], and postoperative pain [7]. Additional benefits include parietal preservation, better cosmetic

outcomes, earlier resumption of physical activity [8], and facilitation of redo surgery [9]. Despite its advantages and increasing usage, LH is offered only at referral centers, with technical difficulties and the necessities for experience in both hepatobiliary and complex laparoscopic surgery hampering its widespread adoption [10]. Although preoperative computer-assisted surgical simulation, such as computed tomography volumetry, has been widely used in daily clinical practice, development of the novel intraoperative systems in computer-assisted surgery (CAS), which help surgeons to perform safer and more efficient procedures like LH, are expected [11].

Abbreviations: AI, artificial intelligence; CAS, computer-assisted surgery; CNN, convolutional neural network; HMM, Hidden Markov model; LH, Laparoscopic hepatectomy; NCCHE, National Cancer Center Hospital East.

* Corresponding author: Surgical Device Innovation Office, National Cancer Center Hospital East, 6-5-1, Kashiwanoha, Kashiwa-City, Chiba, 277-8577, Japan.

E-mail addresses: maito@east.ncc.go.jp, maito@east.ncc.go.jp (M. Ito).

<https://doi.org/10.1016/j.ijso.2022.106856>

Received 21 July 2022; Accepted 19 August 2022

Available online 27 August 2022

1743-9191/© 2022 IJS Publishing Group Ltd. Published by Elsevier Ltd. All rights reserved.

In recent years, automated surgical workflow identification using artificial intelligence (AI) has been performed in minimally invasive surgery [12–15]. Real-time automated surgical step identification, in which AI automatically identifies and judges the operative fields and surgical procedures as one of several pre-defined data in real-time, is a fundamental component for developing intraoperative CAS systems [16]. This real-time automated step identification could be applied to CAS-based clinical decision support systems that may provide real-time useful information to surgeons in relation to the actual step and course of the operation, such as information regarding target lesions that are approaching or adjacent to anatomical landmarks that may be fatal if injured [17]. We expect that intraoperative CAS systems may help to standardize and spread safer procedures in LH. To our knowledge, studies describing automated surgical step identification focused on LH are lacking. Therefore, this study aimed to develop a deep-learning model for automated surgical step identification in LH.

2. Methods

2.1. Creation of the dataset

We constructed a dataset containing 40 cases of pure LH partial resection procedures, all of which were performed by four surgeons at the National Cancer Center Hospital East (NCCHE) in Kashiwa, Japan, between July 2018 and December 2019. All procedures were recorded using a VISERA ELITE system (Olympus Inc., Tokyo, Japan) with a 10-mm camera or a KTH 102 endoscope (Karl Storz Inc., Tuttlingen, Germany) with a 10-mm camera and a 30° angle. During pre-processing, all videos were converted into the same codec (MPEG-4 AVC/H.264) and display resolution (vertical resolution, 720 pixels). The video data were divided into frame units of every 1/30 of a second (30 frames per second) as static images.

All 40 pure LH videos were separated into predetermined surgical workflow patterns, referred to as “surgical steps.” Each video was manually divided into nine surgical steps (Step 0–8), based on the method of task analysis: Step 0 comprised extracorporeal actions; Step 1 comprised port insertion; Step 2 comprised lysis of adhesions; Step 3 comprised identification of the target lesion using laparoscopic ultrasound and marking the resection line; Step 4 comprised encircling of the hepatoduodenal ligaments and hepatic inflow-occlusion; Step 5 comprised mobilization of the liver; Step 6 comprised liver transection; Step 7 comprised specimen extraction and closing of the surgical incision; and Step 8 comprised other actions (e.g., waiting for next hepatic inflow occlusion after releasing the clamp) (Fig. 1). Each step, including its start and end points, was clearly defined based on anatomical position and surgical procedure. Although the order of the surgical steps differed depending on the case, the step in which the corresponding surgical procedure was best applied was annotated for each occasion.

2.2. Automated surgical step identification

For surgical step identification, 30 and 10 videos were randomly assigned to a training dataset (which was what the model is trained on) and test dataset (which was used to see how well that model assesses previously unseen data), respectively [18]. A deep-learning approach was used to classify individual video frames as belonging to one of a pre-learned set of steps. Automated identification of eight steps (Steps 1–8) was performed after Step 0 (extracorporeal actions) frames were excluded from the video (Model 1). The Xception model [19] was used as the convolutional neural network (CNN) architecture and was pre-trained using the ImageNet dataset [20]. Algorithm performance was assessed using holdout validation. Moreover, Steps 1 (port insertion), 7 (specimen extraction and closing of the surgical incision), and 8 (other actions) frames were compiled as “Step IP (Invalid Procedure)” to efficiently identify the surgical step and automated identification of six steps (Steps IP and 2–6) in another model (Model 2). Step IP (invalid

procedure) included procedures that do not directly display progress during the operation as the video frames during this step had similar visual features.

2.3. Evaluation metrics

The evaluation metrics for the model were precision, recall, F1 score (which were used as the metrics for each step), and overall accuracy (which was used for the integrated steps). The F1 score of each class and overall accuracy of all classes were considered the most significant variable in the evaluation of the deep-learning model for classification [20]. The calculation formula for each metric is shown below, where TP represents true positive classifications, FP represents false positive classifications, TN represents true negative classifications, and FN represents false-negative classifications.

$$\text{Precision} = \frac{TP}{TP + FP}$$

$$\text{Recall} = \frac{TP}{TP + FN}$$

$$\text{F1score} = 2 \cdot \frac{\text{Precision} \cdot \text{Recall}}{\text{Precision} + \text{Recall}}$$

$$\text{Overall accuracy} = \frac{TP + TN}{TP + FP + TN + FN}$$

2.4. Real-time automated surgical step identification

Since it takes more time for AI to identify the surgical steps than to capture frames, multi-threading was applied to realize real-time step identification. While one thread of AI captured a frame from a camera device, another thread identified the step using the deep neural network model. When the step identification was completed, the inferred step was updated and displayed in the current frame [12]. The model was trained with a single graphics processing unit with 16 GB of VRAM (Quadro® GP100; Nvidia Inc. Santa Clara, CA, USA), as was the surgical step being tested.

2.5. Ethical declarations

The study protocol was approved by the institutional review board of the NCCHE (registration no. 2020-315). All patients provided written informed consent for this project. This project was conducted in compliance with the Declaration of Helsinki, Ethical Principles for Medical Research Involving Human Subjects (as amended in Fortaleza, October 2013) [21].

3. Results

3.1. The dataset

Table 1 summarizes the baseline patient information for the collected pure LH videos (n = 40). The median patient age was 69.5 years (range, 39–84 years); 22 (55%) patients were male, and their median body mass index was 23.3 kg/m² (range, 14.4–32.5 kg/m²). All patients had Child–Pugh class A lesions. The most common pathological diagnosis of the tumor was colorectal liver metastases (62.5%). In 35 cases (87.5%), the number of resected tumors was one. The median maximum tumor diameter was 15 mm (range, 5–45 mm). The most common tumor location was segment 6 (40.0%). The median operation time was 122 min (range, 38–216 min), and the median blood loss was 36 mL (range, 0–200 mL).

There were 8,119,595 frames in the dataset comprising the 40 pure LH cases, and each frame was labeled with its corresponding surgical step. The duration for each surgical step is shown in Fig. 2. The duration

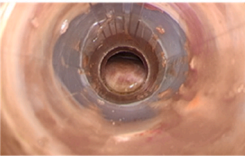
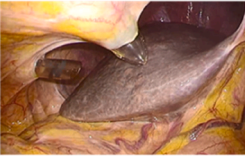
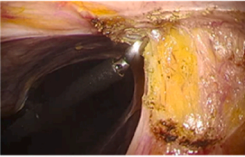

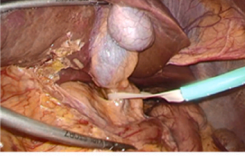
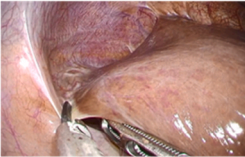

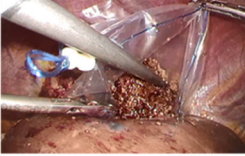
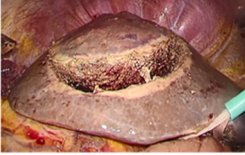
Step	Definition	Representative image	Description
0	Extracorporeal action		Start: The endoscope is removed from the abdominal cavity. End: The endoscope is inserted into the abdominal cavity.
1	Port insertion		Start: The abdominal wall is pushed to allow insertion of the laparoscopic ports. End: The abdominal wall is pushed to allow insertion of the laparoscopic ports.
2	Adhesiotomy		Start: The adhesion around the liver is divided. End: The division is finished.
3	Identifying the lesion using laparoscopic ultrasound and marking the resection line		Start: The laparoscopic ultrasonic probe or acusector appears on the screen. End: The instruments disappear from the screen.
4	Encircling of the hepatoduodenal ligaments and hepatic inflow-occlusion		Start: A tourniquet tube to encircle the hepatoduodenal ligament appears for hepatic inflow occlusion. End: The tube disappears from the screen.
5	Mobilization of the liver		Start: The triangular, coronary, or falciform ligament of the liver is approached by laparoscopic forceps. End: The instrument no longer touched the liver.
6	Liver transection		Start: The liver parenchyma and hepatic vessels are transected. End: The instrument disappears from the screen.
7	Specimen extraction and closing of the surgical incision		Start: The bag appears on the screen. End: end point of the video
8	Other actions (e.g., waiting for next Pringle maneuver after releasing the clamp)		Start: previous step ends End: following step starts

Fig. 1. Definition of the eight surgical steps annotated in the notarized laparoscopic hepatectomy (LH) videos, with representative images and descriptions of their start and end points.

Table 1
Baseline characteristics (n = 40).

Variable	Result
Age, years	69.5 (39–84) ^a
Sex, n (%)	
Male	22 (55%)
Female	18 (45%)
Body mass index, kg/m ²	23.3 (14.4–32.5) ^a
Pathological diagnosis, n (%)	
Colorectal liver metastases	25 (62.5%)
Hepatocellular carcinoma	12 (30%)
Intrahepatic cholangiocellular carcinoma	3 (7.5%)
Number of tumors, n (%)	
1	35 (87.5)
2	5 (12.5)
Tumor location, n (%)	
Segment 4	3 (7.5)
Segment 5	7 (17.5)
Segment 6	16 (40)
Segment 7	2 (5)
Segment 8	12 (30)
Maximum tumor diameter, mm	15 (5–45) ^a
Child-Pugh Score A, n (%)	40 (100)
Indocyanine green R15, %	10.7 (5–68.8) ^a
History of hepatitis, n (%)	
B	3(7.5)
C	4(10)
Alcoholic	1(2.5)
Operation time, min	123 (38–216) ^a
Blood loss, mL	18 (0–200) ^a
Experience of operating surgeons, years	16 (6–21) ^a

^a Median (range).

for Step 6 (liver transection) was the longest and varied most widely between each patient (median, 46 min; range, 10–101 min), whereas Step 2 (lysis of adhesion) occupied the shortest duration (median, 2 min; range, 0–16 min). All eight tagged steps occurred only in 5 of the 40 cases; Step 2 (lysis of adhesion), Step 4 (encircling of the hepatoduodenal ligaments and hepatic inflow occlusion), and Step 5 (mobilization of the liver) were not performed in 22, 2, and 22 cases, respectively.

3.2. Automated surgical step identification

The step identification results of both models are compared to the manually annotated data in a representative case in Fig. 3A. In Model 1, Steps 3 (identification of the target lesion using laparoscopic ultrasound and marking the resection line), 4 (encircling of the hepatoduodenal ligaments and hepatic inflow-occlusion), and 6 (liver transection) were almost correctly identified, which were in contrast to Step 8 (other actions). In Model 2, Steps 1 (port insertion), 7 (specimen extraction and closing of the surgical incision), and 8 (other actions) were compiled as “Step IP (invalid procedure)”. Consequently, Step IP (invalid procedure) was almost correctly identified. The longest period that was not correctly identified was the short period of Step IP during the last part of LH, which was misidentified as Step 6 (liver transection) (Fig. 3B). During that period, no hemorrhage and bile leakage on the liver transection plane was confirmed using the same suction instrument as that for liver transection, during which Step IP was misidentified as Step 6 by AI.

The results of the evaluation metrics in the test dataset are shown in Table 2. The overall accuracy of Model 1 was 0.891, which was increased to 0.947 in Model 2. The median accuracy for each case was 0.879 (range, 0.842–0.947) in Model 1, and 0.927 (range, 0.884–0.997) in Model 2. The average accuracy for each case was 0.890 ± 0.04 (standardized difference; SD) in Model 1 and 0.937 ± 0.04 (SD) in Model 2. The deep-learning model included automated surgical step identification in real-time at 21 frames per second (range, 16–22) on average. The video for automated surgical step identification is shown in Video 1.

Supplementary video related to this article can be found at <https://doi.org/10.1016/j.ijssu.2022.106856>

4. Discussion

This study described the use of AI with deep learning for identifying surgical steps in 40 pure LH cases, based on manually annotated data. The overall accuracy of Model 1 was 0.891, which was increased to 0.947 in Model 2. The SD of accuracy according to each case was only 0.04 in both Models 1 and 2, which indicated that the accuracy of our model was highly consistent across different cases. Real-time automated surgical step identification was achieved at 21 frames per second. Our

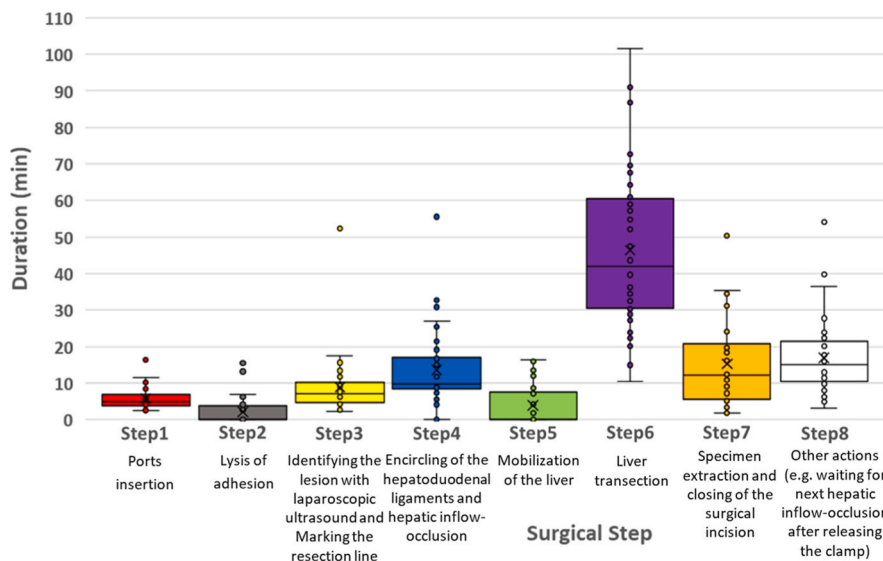


Fig. 2. Box and whisker plot showing duration among the different surgical steps. The boundary of the box closest to zero indicates the 25th percentile, the black cross mark within the box marks the median, and the boundary of the box farthest from zero indicates the 75th percentile. Whiskers above and below the box indicate the 10th and 90th percentiles. Points above and below the whiskers indicate outliers outside the 10th and 90th percentiles.

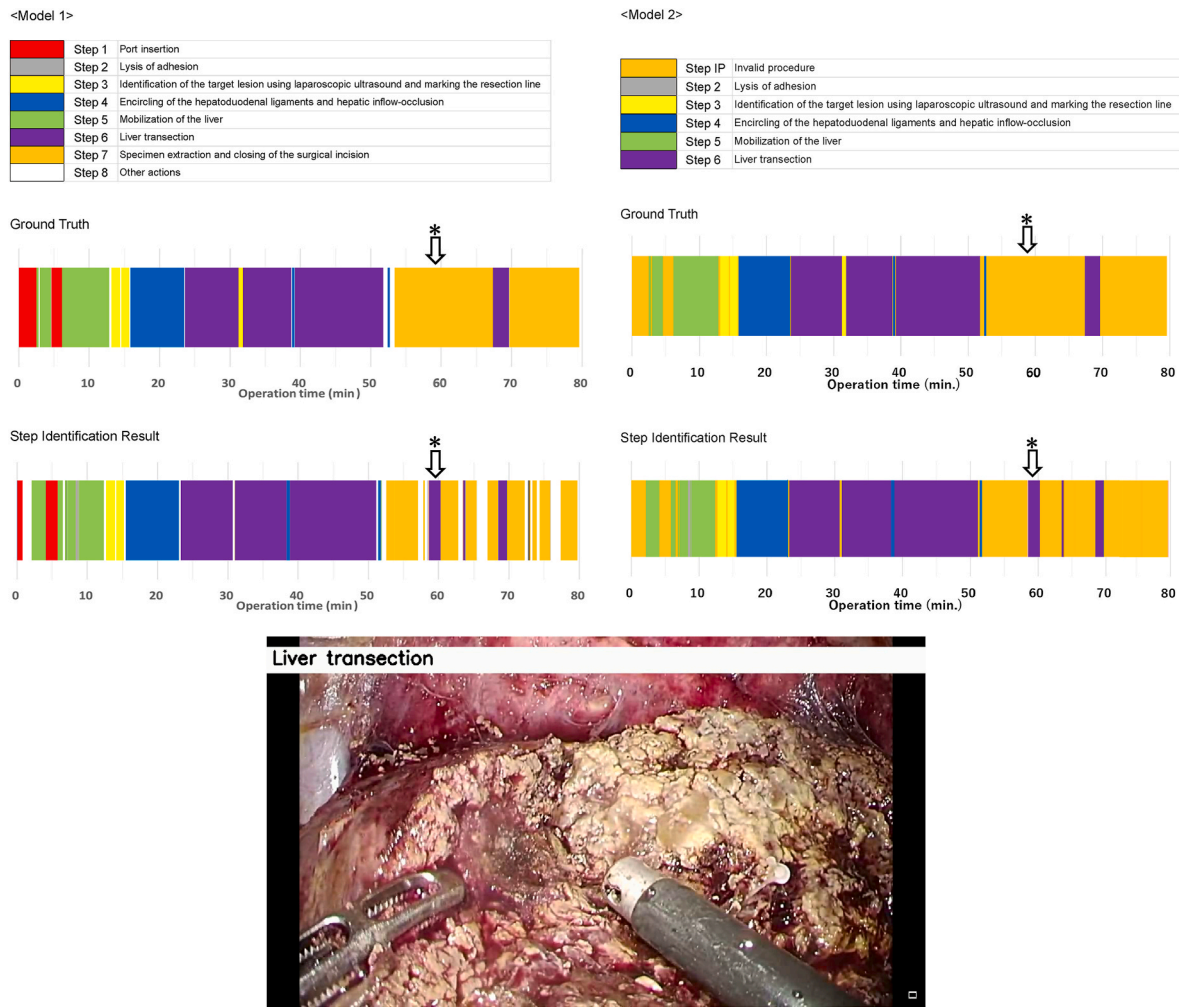


Fig. 3. A. Comparison of the step identification results and a surgeon-notarized video for a representative case from the LH dataset in a color-coded ribbon illustration. The top ribbon shows the surgeon-notarized video, wherein data which was labeled manually. The bottom ribbon indicates the duration of the predicted step. A short period for Step IP (*) in the surgeon-notarized video was misidentified as Step 6 by AI, in which a representative scene was captured as Fig. 3B. B. The scene which Step IP was misidentified as Step 6 by AI. During this period, no hemorrhage and bile leakage within the liver transection plane was confirmed using the same suction instrument as that for liver transection. (For interpretation of the references to color in this figure legend, the reader is referred to the Web version of this article.)

Table 2
Precision, recall, and F1 scores for automated surgical step identification.

Step	Model 1			Model 2		
	Precision	Recall	F1 score	Precision	Recall	F1 score
1 Port insertion	0.819	0.745	0.780	Not applicable		
2 Lysis of adhesion	0.905	0.959	0.931	0.905	0.959	0.931
3 Identification of the target lesion using laparoscopic ultrasound and marking of the resection line	0.961	0.919	0.939	0.961	0.919	0.939
4 Encircling of the hepatoduodenal ligaments and hepatic inflow occlusion	0.899	0.934	0.916	0.899	0.934	0.916
5 Mobilization of the liver	0.947	0.937	0.942	0.947	0.937	0.942
6 Liver transection	0.960	0.974	0.967	0.960	0.974	0.967
7 Specimen extraction and closing of the surgical incision	0.828	0.726	0.774	Not applicable		
8 Other actions	0.564	0.596	0.579	Not applicable		
IP: Invalid Procedure	Not applicable			0.899	0.866	0.882
Overall accuracy	0.891			0.937		
Accuracy of each case, median (range)	0.879 (0.842–0.947)			0.927 (0.884–0.997)		
average ± standard deviation	0.890 ± 0.04			0.937 ± 0.04		

results showed that real-time automated surgical step identification with a high frame rate is feasible and that our deep-learning model facilitated automated video indexing. To the best of our knowledge, this is the first study in which a deep-learning based classification approach was applied to a video dataset of LH cases.

Recently, a deep-learning model of automated surgical step identification has been reported in several procedures, such as laparoscopic sigmoidectomy (LS), cholecystectomy, and gastrectomy [12–15]. The reported data on overall accuracy ranged from 0.728 to 0.919. In contrast, our model for LH achieved a higher overall accuracy (0.891 in

Model 1 and 0.947 in Model 2). We consider that there were mainly two reasons for the unexceptionally high accuracy of our model. First, we achieved high accuracy by compiling three steps into “Step IP (Invalid Procedure)” in Model 2. Step IP is composed of Steps 1 (port insertion), 7 (specimen extraction and closing of the surgical incision), and 8 (other actions). These steps included procedures that do not directly visually show progress during the operation. Additionally, the video frames in these steps have similar visual features, and it is difficult for the model to distinguish them accurately. Therefore, by compiling these three steps into a “Step IP”, we succeeded to develop not only a highly accurate deep-learning model but also a model that effectively identified the essential surgical parts during LH. Second, the high accuracy of our model may reflect the mechanism of the utilized computer vision techniques to identify surgical steps in laparoscopic videos. A deep-learning model automatically learns the visual features of every frame from the training dataset. The model then identifies the surgical step in the test dataset based on these identified visual features [22]. In LH, the visual features of the targeted structures differ clearly (e.g., liver capsule, liver parenchyma, intra-corporeal fat in the abdomen), as do the specific instruments used during each surgical step (e.g., intraoperative ultrasonic probe in Step 3, tourniquet tube for the hepatic inflow occlusion in Step 4). These characteristic features of liver anatomy and surgical instruments during LH may help AI to distinguish surgical steps from each other. On the contrary, it may be difficult for AI to correctly recognize each surgical step during LS because the colon is naturally difficult to distinguish from the rectum and no characteristic surgical instruments are used during each surgical step. Therefore, we consider that LH may be more suitable for CAS systems to identify surgical steps than LS and other operations.

As for our future perspective, our deep-learning model could serve as a basis for CAS to provide real-time information during LH in the operative field. For example, our model provides real-time updates regarding procedure progress, helps guide the use of surgical instruments for assistants and surgical teams, and estimates the remaining duration of surgery, which will improve the efficiency of operating room usage [12–15]. Second, our model could be applied to the hospital system to create informative and focused education material for surgical trainees. Our model automatically understands surgical images, and it could be utilized to help identify specific segments of an operation to help make video reviews more efficient. Third, our model has already identified liver transection, and this model will be improved in the future to automatically identify bleeding within the parenchymal dissection plane, which may eventually contribute to increased patient safety during LH. We believe that our model of automatic surgical step identification using AI will contribute to developing intraoperative CAS systems in the future that effectively arrange operating room logistics and help surgeons perform LH with more ease.

The main limitation of the present study was the similarity of the videos within the dataset. Videos were procured from a single institution; therefore, the complexity of the data was limited. Training a deep-learning model with a limited dataset can lead to over-fitting and consequent loss of generalizability [23]. During LH, various surgical procedures, including major hepatectomy were performed, and different characteristic surgical instruments, such as intraoperative laparoscopic ultrasonography, ultrasonic dissection, and laparoscopic coagulating shears released by various companies, were used by different institutions [24]. This variety of procedures and instruments may decrease the accuracy of our model if applied to videos from other institutions. However, we considered that our model would be able to obtain more accurate and generalizable networks by increasing the number and variation of LH videos. We are now constructing a large dataset containing 300 LH videos obtained from high-volume endoscopic centers in Japan as a project of the Japan Agency for Medical Research and Development [25]. We consider that this new model, which is developed from a large dataset would resolve some above-stated limitations. Even if LH from other institutions vary regarding procedures and surgical

instruments, the visual features of the specific instruments used during each surgical step also differ clearly. By using training data, including videos from other institutions, this new model could accurately identify surgical steps in various LH cases. A further limitation was that the performance of our model was still insufficient for clinical applications. EndoBRAIN® (Olympus Inc., Tokyo, Japan), an automated identification system of colorectal neoplasms using AI in endoscopy, had obtained regulatory approval of medical device and has been released to the market in Japan in 2019 [26]. The first report of that system was published in 2018 and the accuracy of automated identification was 0.765 [27]. Afterward, the system had been trained by increasing both the number and variation of cases, utilizing multiple medical institutions. Only then did the accuracy of the system improve [28]. Therefore, by increasing the number and variation of data, we consider that our model will achieve higher accuracy.

Another limitation of the present study was annotation granularity. Our annotation schema, with its nine labels, only captured big-picture steps of LH, which does not account for the smaller sub-components. “Step 6 (liver transection),” for example, could be split into “transection of the hepatic capsule,” “transection of liver parenchyma,” and “exposure, clipping, and dissection of vessels or ducts.” A more granular annotation structure would create a foundation for advanced warning prior to adverse events (like bleeding from a vessel) and provide meaningful intra-operative findings to guide post-operative risk prediction [29]. However, increased annotation granularity presents difficulties for current deep-learning technology because it leads to shorter temporal segments. Although less training data and training optimization for overall accuracy make it difficult for AI to identify short duration steps, newer approaches of deep-learning, such as the Hidden Markov model (HMM) approach, have been tried to resolve this problem [30]. With improved model design and the new annotation standard, AI can perform granular step identification, and this would provide well-detailed information to develop further valuable CAS systems for LH.

5. Conclusion

We developed a highly accurate deep-learning model for surgical step identification in pure laparoscopic hepatectomy. Our model could be applied to various systems of computer-assisted surgery.

Provenance and peer review

Not commissioned, externally peer-reviewed.

Disclosure information

All authors have no financial conflicts of interest to disclose concerning this research.

Role of the funding source

This research was supported by the Japan Agency for Medical Research and Development (grant number JP 20he2102001h0002).

Author contributions

Study conception and design: Sasaki, Ito, Takeshita.
 Acquisition of data: Sasaki, Kobayashi, Gotohda.
 Analysis and interpretation of data: Sasaki, Matsuzaki, Takeshita.
 Drafting of manuscript: Sasaki.
 Critical revision: Ito, Kitaguchi, Kudo, Hasegawa, Sugimoto, Mitsunaga, Gotohda.

Acknowledgments

None.

References

- [1] H. Reich, F. McGlynn, J. DeCaprio, R. Budin, Laparoscopic excision of benign liver lesions, *Obstet. Gynecol.* 78 (1991) 956–958.
- [2] J.F. Buell, D. Cherqui, D.A. Geller, et al., The international position on laparoscopic liver surgery: the Louisville Statement, *Ann. Surg.* 250 (2009) (2008) 825–830, <https://doi.org/10.1097/sla.0b013e3181b3b2d8>.
- [3] D. Ban, M. Tanabe, H. Kumamaru, et al., Safe dissemination of laparoscopic liver resection in 27,146 cases between 2011 and 2017 from the national clinical database of Japan, *Ann. Surg.* 274 (2021) 1043–1050, <https://doi.org/10.1097/SLA.0000000000003799>.
- [4] G. Wakabayashi, D. Cherqui, D.A. Geller, et al., Recommendations for laparoscopic liver resection: a report from the second international consensus conference held in Morioka, *Ann. Surg.* 261 (2015) 619–629, <https://doi.org/10.1097/SLA.0000000000001184>.
- [5] M. Kasai, F. Cipriani, B. Gayet, et al., Laparoscopic versus open major hepatectomy: a systematic review and meta-analysis of individual patient data, *Surgery* 163 (2018) 985–995, <https://doi.org/10.1016/j.surg.2018.01.020>.
- [6] H. Tranchart, G. Di Giuro, P. Lainas, et al., Laparoscopic resection for hepatocellular carcinoma: a matched-pair comparative study, *Surg. Endosc.* 24 (2010) 1170–1176, <https://doi.org/10.1007/s00464-009-0745-3>.
- [7] I. Dagher, G. Di Giuro, J. Dubrez, et al., Laparoscopic versus open right hepatectomy: a comparative study, *Am. J. Surg.* 198 (2009) 173–177, <https://doi.org/10.1016/j.amjsurg.2008.09.015>.
- [8] M. Gagner, T. Rogula, D. Selzer, Laparoscopic liver resection: benefits and controversies, *Surg. Clin. Clin.* 84 (2004) 451–462, <https://doi.org/10.1016/j.suc.2003.11.002>.
- [9] G. Belli, L. Cioffi, C. Fantini, et al., Laparoscopic redo surgery for recurrent hepatocellular carcinoma in cirrhotic patients: feasibility, safety, and results, *Surg. Endosc.* 23 (2009) 1807–1811, <https://doi.org/10.1007/s00464-009-0344-3>.
- [10] A. Radtke, G.C. Sotiropoulos, E.P. Molmenti, et al., Computer-assisted surgery planning for complex liver resections: when is it helpful? A single-center experience over an 8-year period, *Ann. Surg.* 252 (2010) 876–883, <https://doi.org/10.1097/SLA.0b013e3181fdd012>.
- [11] A. Zygomalas, I. Kehagias, Up-to-Date Intraoperative Computer Assisted Solutions for Liver Surgery, *World J Gastrointest Surg* Baishideng Publishing Group Inc., 2019, pp. 1–10.
- [12] A.P. Twinanda, G. Yengera, D. Mutter, et al., RSDNet: learning to predict remaining surgery duration from laparoscopic videos without manual annotations, *IEEE Trans. Med. Imag.* 38 (2019) 1069–1078, <https://doi.org/10.1109/TMI.2018.2878055>. →18–21.
- [13] D.A. Hashimoto, G. Rosman, E.R. Witkowski, et al., Computer vision analysis of intraoperative video: automated recognition of operative steps in laparoscopic sleeve gastrectomy, *Ann. Surg.* 270 (2019) 414–421, <https://doi.org/10.1097/SLA.0000000000003460>.
- [14] D. Kitaguchi, N. Takeshita, H. Matsuzaki, et al., Real-time automatic surgical phase recognition in laparoscopic sigmoidectomy using the convolutional neural network-based deep learning approach, *Surg. Endosc.* 34 (2020) 4924–4931, <https://doi.org/10.1007/s00464-019-07281-0>.
- [15] D. Kitaguchi, N. Takeshita, H. Matsuzaki, et al., Automated laparoscopic colorectal surgery workflow recognition using artificial intelligence: experimental research, *Int. J. Surg.* 79 (2020) 88–94, <https://doi.org/10.1016/j.ijso.2020.05.015>.
- [16] F. Lalys, P. Jannin, Surgical process modelling: a review, *Int. J. Comput. Assist. Radiol. Surg.* 9 (2014) 495–511, <https://doi.org/10.1007/s11548-013-0940-5>.
- [17] C.R. Garrow BSc, K.F. Kowalewski, L. Li BSc, et al., Machine learning for surgical phase recognition: a Systematic Review, 2021– 273, *Ann. Surg.* April 273 (4) (2021) 684–693, <https://doi.org/10.1097/SLA.0000000000004425>, 684–693.
- [18] G.I. Sammut C Webb (Ed.), *Hold Out Evaluation, Encyclopedia of Machine Learning and Data Mining*, Springer, 2017, 624–624.
- [19] C.F. Xception, Deep learning with depthwise separable convolutions, *CVPR* (2017) 1800–1807, 2017.
- [20] A. Krizhevsky, I. Sutskever, G.E. Hinton, ImageNet classification with deep convolutional neural networks, *Commun. ACM* 60 (2017) 84–90, <https://doi.org/10.1145/3065386>. <https://dl.acm.org/doi/10.1145/3065386>.
- [21] World Medical Association, World Medical Association declaration of Helsinki: ethical principles for medical research involving human subjects, *JAMA* 310 (2013) 2191–2194, <https://doi.org/10.1001/jama.2013.281053>.
- [22] A.P. Twinanda, S. Shehata, D. Mutter, et al., EndoNet: a deep architecture for recognition tasks on laparoscopic videos, *IEEE Trans. Med. Imag.* 36 (2017) 86–97, <https://doi.org/10.1109/TMI.2016.2593957>.
- [23] H. Liu, Z.H. Mo, H. Yang, et al., Automatic facial recognition of Williams-Beuren syndrome based on deep convolutional neural networks, *Front. Pediatr.* 9 (2021), 648255, <https://doi.org/10.3389/fped.2021.648255>.
- [24] H. Kaneko, Y. Otsuka, M. Tsuchiya, et al., Application of devices for safe laparoscopic hepatectomy, *HPB* 10 (2008) 219–224, <https://doi.org/10.1080/13651820802166831>.
- [25] Japan Agency for Medical Development, (AMED), Title of Research, Development of a transversal infrastructure for building a database of endoscopic surgery, Grant Number JP 20he2102001h0002, https://amedfind.amed.go.jp/amed/search/tas_k_search_details.html.
- [26] PRESS RELEASE EndoBRAIN®-EYE, AI-equipped colorectal endoscopy diagnosis support software Part 2. Acquisition of Approval under Pharmaceutical and Medical Device Act (PMD Act) EndoBRAIN®-EYE, software to support diagnosis in colorectal endoscopy using artificial intelligence (AI). <https://www.cybernet.jp/english/documents/pdf/news/press/2020/20200129.pdf>, 2020.
- [27] M. Misawa, S. ei Kudo, Y. Mori, et al., Artificial intelligence-assisted polyp detection for colonoscopy: initial experience, *Gastroenterology* 154 (2018) 2027–2029, e3.
- [28] S. ei Kudo, M. Misawa, Y. Mori, et al., Artificial intelligence-assisted system improves endoscopic identification of colorectal neoplasms, *Clin. Gastroenterol. Hepatol.* 18 (2020) 1874–1881, e2.
- [29] T.M. Ward, D.A. Hashimoto, Y. Ban, et al., Automated operative phase identification in peroral endoscopic myotomy, *Surg. Endosc.* 35 (2021) 4008–4015, <https://doi.org/10.1007/s00464-020-07833-9>.
- [30] Y. Jin, Q. Dou, H. Chen, et al., SV-RCNet: workflow recognition from surgical videos using recurrent convolutional network, *IEEE Trans. Med. Imag.* 37 (2018) 1114–1126, <https://doi.org/10.1109/TMI.2017.2787657>.